

# The MAJORANA DEMONSTRATOR calibration system

N. Abgrall<sup>a</sup>, I.J. Arnquist<sup>b</sup>, F.T. Avignone III<sup>c,d</sup>, A.S. Barabash<sup>e</sup>, F.E. Bertrand<sup>d</sup>, M. Boswell<sup>f</sup>, A.W. Bradley<sup>a</sup>, V. Brudanin<sup>g</sup>, M. Busch<sup>h,i</sup>, M. Buuck<sup>j</sup>, T.S. Caldwell<sup>k,i</sup>, C.D. Christofferson<sup>l</sup>, P.-H. Chu<sup>f</sup>, C. Cuesta<sup>j</sup>, J.A. Detwiler<sup>j</sup>, C. Dunagan<sup>l</sup>, Yu. Efremenko<sup>m</sup>, H. Ejiri<sup>n</sup>, S.R. Elliott<sup>f</sup>, Z. Fu<sup>j</sup>, V.M. Gehman<sup>f</sup>, T. Gilliss<sup>k,i</sup>, G.K. Giovanetti<sup>p</sup>, J. Goett<sup>f</sup>, M.P. Green<sup>o,i,d</sup>, J. Gruszko<sup>j</sup>, I.S. Guinn<sup>j</sup>, V.E. Guiseppe<sup>c</sup>, C.R. Haufe<sup>k,i</sup>, R. Henning<sup>k,i</sup>, E.W. Hoppe<sup>b</sup>, M.A. Howe<sup>k,i</sup>, B.R. Jasinski<sup>q</sup>, K.J. Keeter<sup>r</sup>, M.F. Kidd<sup>s</sup>, S.I. Konovalov<sup>e</sup>, R.T. Kouzes<sup>b</sup>, A.M. Lopez<sup>m</sup>, J. MacMullin<sup>k,i</sup>, R.D. Martin<sup>t</sup>, R. Massarczyk<sup>f,\*</sup>, S.J. Meijer<sup>k,i</sup>, S. Mertens<sup>a</sup>, J.L. Orrell<sup>b</sup>, C. O'Shaughnessy<sup>k,i</sup>, A.W.P. Poon<sup>a</sup>, D.C. Radford<sup>d</sup>, J. Rager<sup>k,i</sup>, A.L. Reine<sup>k,i</sup>, K. Rielage<sup>f</sup>, R.G.H. Robertson<sup>j</sup>, B. Shanks<sup>k,i</sup>, M. Shirchenko<sup>g</sup>, A.M. Suriano<sup>l</sup>, D. Tedeschi<sup>c</sup>, J.E. Trimble<sup>k,i</sup>, R.L. Varner<sup>d</sup>, S. Vasilyev<sup>g</sup>, K. Vetter<sup>a,1</sup>, K. Vorren<sup>k,i</sup>, B.R. White<sup>f</sup>, J.F. Wilkerson<sup>k,i,d</sup>, C. Wiseman<sup>c</sup>, W. Xu<sup>q</sup>, C.-H. Yu<sup>d</sup>, V. Yumatov<sup>e</sup>, I. Zhitnikov<sup>g</sup>, B.X. Zhu<sup>f</sup>

<sup>a</sup>Nuclear Science Division, Lawrence Berkeley National Laboratory, Berkeley, CA, USA

<sup>b</sup>Pacific Northwest National Laboratory, Richland, WA, USA

<sup>c</sup>Department of Physics and Astronomy, University of South Carolina, Columbia, SC, USA

<sup>d</sup>Oak Ridge National Laboratory, Oak Ridge, TN, USA

<sup>e</sup>National Research Center "Kurchatov Institute" Institute for Theoretical and Experimental Physics, Moscow, Russia

<sup>f</sup>Los Alamos National Laboratory, Los Alamos, NM, USA

<sup>g</sup>Joint Institute for Nuclear Research, Dubna, Russia

<sup>h</sup>Department of Physics, Duke University, Durham, NC, USA

<sup>i</sup>Triangle Universities Nuclear Laboratory, Durham, NC, USA

<sup>j</sup>Center for Experimental Nuclear Physics and Astrophysics, and Department of Physics, University of Washington, Seattle, WA, USA

<sup>k</sup>Department of Physics and Astronomy, University of North Carolina, Chapel Hill, NC, USA

<sup>l</sup>South Dakota School of Mines and Technology, Rapid City, SD, USA

<sup>m</sup>Department of Physics and Astronomy, University of Tennessee, Knoxville, TN, USA

<sup>n</sup>Research Center for Nuclear Physics and Department of Physics, Osaka University, Ibaraki, Osaka, Japan

<sup>o</sup>Department of Physics, North Carolina State University, Raleigh, NC, USA

<sup>p</sup>Department of Physics, Princeton University, Princeton, NJ, USA

<sup>q</sup>Department of Physics, University of South Dakota, Vermillion, SD, USA

<sup>r</sup>Department of Physics, Black Hills State University, Spearfish, SD, USA

<sup>s</sup>Tennessee Tech University, Cookeville, TN, USA

<sup>t</sup>Department of Physics, Engineering Physics and Astronomy, Queen's University, Kingston, ON, Canada

arXiv:1702.02466v1 [physics.ins-det] 7 Feb 2017

## Abstract

The MAJORANA Collaboration is searching for the neutrinoless double-beta decay of the nucleus  $^{76}\text{Ge}$ . The MAJORANA DEMONSTRATOR is an array of germanium detectors deployed with the aim of implementing background reduction techniques suitable for a 1-tonne  $^{76}\text{Ge}$ -based search. The ultra low-background conditions require regular calibrations to verify proper function of the detectors. Radioactive line sources can be deployed around the cryostats containing the detectors for regular energy calibrations. When measuring in low-background mode, these line sources have to be stored outside the shielding so they do not contribute to the background. The deployment and the retraction of the source are designed to be controlled by the data acquisition system and do not require any direct human interaction. In this paper, we detail the design requirements and implementation of the calibration apparatus, which provides the event rates needed to define the pulse-shape cuts and energy calibration used in the final analysis as well as data that can be compared to simulations.

**Keywords:** neutrinoless double-beta decay, germanium detector, Majorana, detector calibration

## 1. Introduction

Neutrinoless double-beta decay ( $0\nu\beta\beta$ ) is a hypothesized yet unobserved second order process not permitted by the Standard Model. Such a second order weak process would violate lepton number conservation [1, 2]. Completed searches to date and first results from running experiments [3, 4, 5, 6] indicate half

lives extending beyond  $10^{25}$  years. If this process were to be observed experimentally, it would signal the Majorana nature of the neutrinos and indicate a violation of the lepton number. Through sphaleron processes in the early universe, the violation of baryon number would then result, a necessary condition and explanation for the present-day matter excess over antimatter in the universe [7].

The MAJORANA DEMONSTRATOR (MJD) [8] is a research and development effort aimed at deploying novel background reduction techniques. Such techniques are needed to build a 1-ton experiment with a projected background rate after analysis cuts

\*Corresponding author

Email address: massarczyk@lanl.gov (R. Massarczyk)

<sup>1</sup>Alternate Address: Department of Nuclear Engineering, University of California, Berkeley, CA, USA

of less than 1 count/(ROI tonne year) at the Q-value of the  $0\nu\beta\beta$  decay at 2039 keV. This is accomplished by fielding an array of highly enriched p-type point contact (PPC) Ge detectors underground at the 4850 ft level of the Sanford Underground Research Facility with special attention to the radio-purity of materials in the environment surrounding the Ge detectors. The array is divided into two cryostats, each containing 7 strings of 4 or 5 detectors. Each of the two cryostats has its own vacuum and cooling system. These independent assemblies are referred to as Modules 1 and 2. Twenty nine kg of the detectors are made of enriched Ge material that is enriched to  $>87\%$  in  $^{76}\text{Ge}$  and 15 kg from natural Ge. In this paper, we describe the design requirements and implementation of a system for calibrating the detectors in energy and providing high statistics samples for pulse-shape analysis.

## 2. Requirements and design

The calibration system must provide events from a known radioactive source to each detector in the array in about an hour long data set. This ensures that regular calibrations do not significantly reduce the amount of live time needed for the physics program of the DEMONSTRATOR. The current MJD commissioning and data-taking plan foresees one to two weekly calibrations. The dynamic range of the germanium detector and the attached read-out chain goes from sub keV up to 3 MeV in high gain channels and from about 10 keV to 10 MeV in low gain channels. Our region of interest (ROI) is a 3-keV window at 2039 keV, which is the Q-value of a neutrinoless double-beta decay for  $^{76}\text{Ge}$ . Therefore, a  $^{228}\text{Th}$  source is suitable for energy calibration using regions below and above the ROI. Furthermore, it provides peaks for energy calibration at lower energies, which is important for the analysis and the understanding of the background spectrum. Such a source produces gamma rays with a variety of energies. The intensity and relative location of the full-energy peaks, see Table 1, are used to provide a reliable energy calibration for low energies using Pb x-rays around 80 keV as well as at higher energies using the  $^{208}\text{Tl}$  line at 2614 keV. For this highest energy, we aim for the uncertainty in the number of events in the full-energy peak to be less than 1%, so that fits of the peak shape allow an accurate determination of the energy. Adequate statistics during one calibration are determined by the number of events in the  $^{228}\text{Th}$  decay chain peaks. Its 1.9-yr half-life is sufficient to provide enough statistics even through the end of MJD operations to periodically evaluate pulse-shape cut efficiencies and detector stability.

Since multiple energy depositions in a single detector (multi-site events) can sum to energies in our region of interest, we are making use of the unique pulse shape discrimination abilities of PPC detectors to identify single and multi-site events [9, 10]. Hence additional requirement is the provision of enough data to test the efficiency of pulse-shape discrimination cuts in the final analysis. The gain of Ge detectors is generally stable, and can be monitored closely via use of an external pulser. However,

Energy (keV)	isotope	intensity per decay
238.63	$^{212}\text{Pb}$	0.433
240.99	$^{224}\text{Ra}$	0.041
277.36	$^{208}\text{Tl}$	0.023
300.09	$^{212}\text{Pb}$	0.032
583.19	$^{208}\text{Tl}$	0.304
727.33	$^{212}\text{Bi}$	0.065
785.37	$^{212}\text{Bi}$	0.011
860.56	$^{208}\text{Tl}$	0.044
2614.53	$^{208}\text{Tl}$	0.356

Table 1: Overview on most important gamma energies used for MJD calibration. The single and double-escape peak of the 2614-keV line are used as a test for single-site and multi-site events

a regular calibration provides an additional cross-check of the long-term stability of the setup. Detector resolution as well as linearity are monitored by calibration runs.

In addition to basic physics requirements, we are technically limited to a total event rate that can be handled by the front end electronics without excessive pileup. The characteristic slow charge collection of point contact detectors, which makes pulse-shape discrimination possible, in conjunction with the resistive feedback of our front end, limits the allowed event rate to roughly 100 Hz per detector. Detectors on the outermost circumference of the array lie closer to any source deployed around the vacuum cryostat and see a higher rate than those in the center. Therefore, a compromise must be struck between source activity, the position and extent of the source, and the time allotted for calibration runs.

The modular design of the MJD cryostats in combination with the general construction approach have led us to adopt a line source that is deployed through the DEMONSTRATOR's Pb and Cu shielding in a helical track that surrounds each cryostat module, see Figs. 1, 2 and 3. In such a design, the radioactive material is distributed along a cylindrical line-shaped container which can be moved along a track.

The results of a Geant4 [11] simulation were used to determine the optimum source geometry and activity. The simulations considered different choices of pitch angle for a source along a helical path around the cryostat. Results indicated that shielding and symmetry considerations produce roughly equivalent rates in the external detectors, and the driving consideration becomes the event rate in the central strings. Though the solid-angle exposure to the source is consistent for all detectors of an array, there is a greater shielding effect to the top and bottom center detectors, see Fig. 2. Variations in detector dimension across the range of our available detector sizes had a negligible effect on event rate. For this analysis the double-escape peak of the 2614-keV line in  $^{208}\text{Tl}$  is used which is part of the decay chain of  $^{228}\text{Th}$ . From the simulations [12] we conclude that calibration runs should contain at least 400 events in this double-escape peak (as a proxy for the single site analogue for  $0\nu\beta\beta$ ) to validate the pulse-shape cut efficiency. To understand the behaviour and the relative number of single-escape gamma lines in the Compton shoulder, a  $^{60}\text{Co}$  source is used in the commis-

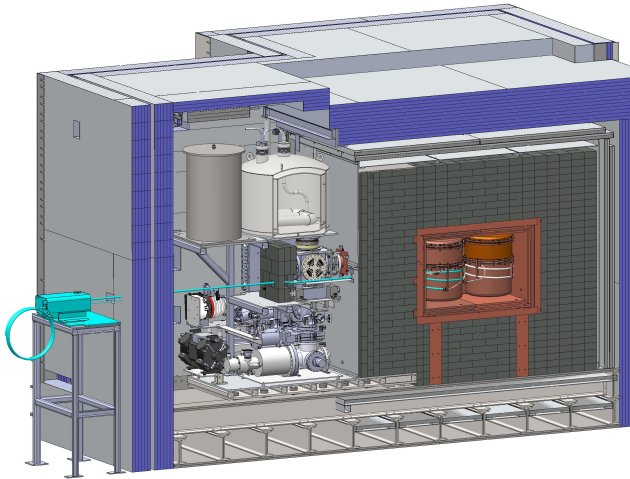


Figure 1: Drawing of a MAJORANA module assembly with calibration system at final position, including the support structure, the vacuum system, nitrogen supply as well as the shielding layers. The loops of the track of Module 2 calibration are visible in cyan. The calibration controls are next to it under the cover next to the loops of the outer storage track.

sioning phase. With the maximum rate in the outer detectors a thorium source of  $\sim 10$  kBq is needed so that the sufficient number of events can be reached in calibration data set of roughly one hour in length.

### 3. Mechanical implementation

#### 3.1. Radioactive line sources

Each line source consists of a radioactively-doped epoxy injected into a 3-mm-diameter tube that is sealed at both ends, produced to our custom specifications by Eckert & Ziegler Analytics, Inc<sup>2</sup>. The source activities are conveniently tuned at production; once cured, can be treated as a sealed source. Deviations from homogeneity along the length of the source are below 3%. Four  $^{228}\text{Th}$  calibration sources were prepared in 1-meter lengths, each with an integrated activity of  $5.18 \pm 0.30$  kBq. A single  $^{60}\text{Co}$  source for building the PSA library was prepared with an integrated activity of  $6.3 \pm 0.30$  kBq over a 2 meter length. The  $^{60}\text{Co}$  source can be exchanged between the two MJD modules at their respective commissioning times. In the final configuration, we fabricated 3 line-source assemblies: one that consists of only the  $^{60}\text{Co}$  source and two assemblies each consisting of a pair of  $^{228}\text{Th}$  sources. For each module only one source at a time can be used.

For positioning purposes, a series of 5-mm long NdFeB grade N42 magnetic slugs are embedded in the source tubing, one pair at the front end of the source, and a second pair with a different spacing between the magnets at the trailing end. The positions of these magnets could be sensed by Hall-effect devices located outside the tubing. Inside the line-source assembly the position of the source containers and magnets

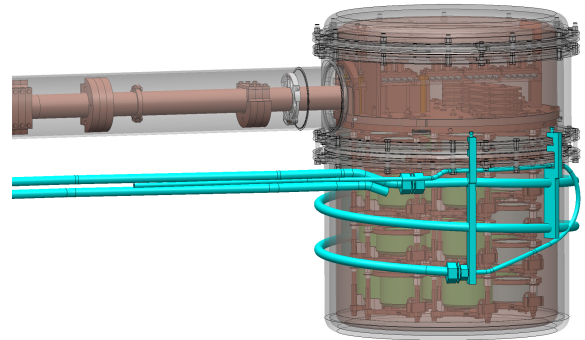


Figure 2: Close-up of the drawing in Fig.1 which shows the relative location of detector array and calibration module.

are fixed using epoxy. The wall thickness of the outer Teflon containment which encapsulates the source material and the magnets is 0.25 mm. The container has been leached in agreement with the MJD cleanliness procedures [13]. During the cleaning steps, a leach removes surface contamination and ensures in case of abrasions of the tube material, no radioactive contamination remains close to the detectors. The total as-built length of a line source assembly is about 4.7 meters.

#### 3.2. Cleanliness

The MJD shield consists of several layers of different shielding material. Electro-formed copper, commercial copper, lead and poly complete the shielding and protect the detectors against radiation of natural origin. A radon exclusion box covers the inner three layers and is purged at all times with boiled-off nitrogen. Around this, two layers of plastic scintillator are used as an active muon veto. The calibration source has to pass through all of these layers; its support structure is located outside the shielding behind the poly shield, see Fig.1. The line source assembly moves in a purged track around the cryostat. This track is made of polytetrafluoroethylene (PTFE). It was assayed in the MJD assay program and leached prior to installation. The chosen PTFE<sup>3</sup> has a very small natural radioactivity with mass fractions below  $3.1 \cdot 10^{-12}$  for  $^{238}\text{U}$  and around  $1.5 \cdot 10^{-12}$  for  $^{232}\text{Th}$ . Inside the shielding, a nitrogen purge line is attached at the inner end to the track and is actively purging the whole track at all times preventing radon intrusion. The entire track forms a closed volume that passes through the different layers of shielding and the veto panels. The end of the track laying outside the shielding is closed by a pneumatic gate valve when no source is deployed, which is installed on the plate indicated in Fig.4. The closed track volume, in combination with the active purge, prevents lab air

<sup>2</sup><http://www.ezag.com/home/>

<sup>3</sup><http://www.coleparmer.com>



Figure 3: Inner calibration track around Module 1. The 1/4-inch-purge line is attached to the 1/2-inch calibration track.

from backfilling the calibration track. Two light emitter and detector pairs are placed on the outside of the gate valve. One pair is used to check the status of the gate valve, while the other pair is used to verify that the radioactive line source is fully retracted behind the valve in its storage position before closing the valve. An improper closing of the valve could damage the thin-walled line source and in the worst case lead to a contamination of radioactive material.

### 3.3. Source positioning

Inside the inner copper shielding, the track is wrapped in a helical shape around the cryostat. The tubing is held in place by clean electro-formed copper brackets which are attached to the cryostat. Figure 3 shows the as-built configuration of the track around one module before it is moved into the shielding. The source itself is guided through small tubing between two drive rollers, cf Fig. 5. One of the drive rollers is rotated by a motor. The second drive roller passively rotates on an axle below the first one. The axle is pulled by two springs against the actively rotating drive roller so that the line source is gently clamped in-between the two drive rollers. This ensures a long-term grip of the drive rollers on the line source.

A deployed source wraps twice around the cryostat allowing a simultaneous calibration of all detectors, in contrast to for example the calibration system of GERDA [14]. Simulations have shown that individual detector rates are highly sensitive to a source's position within the track. More specifically, detector rates are heavily dependent on how far into the helical track a source is deployed. To reproduce the source position more reliably, we have developed a positioning system using Hall effect switches<sup>4</sup>. Three magnetic sensors, see Fig. 4, are connected to an Arduino UNO<sup>5</sup>. These sensors register a passing magnet in a moving line source via the Hall effect. By reading their signal continuously, the arrangement of three sensors outside

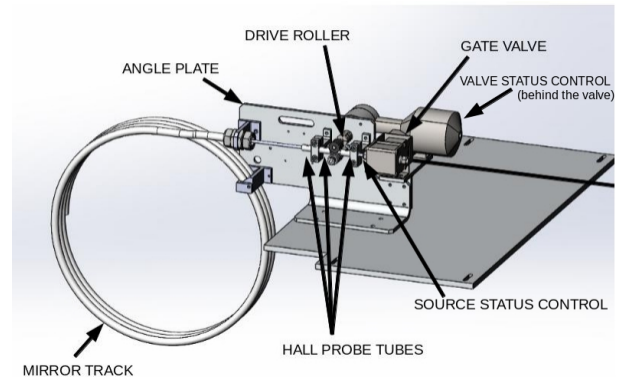


Figure 4: Schematic overview of the sensors installed at the angle plate of the calibration system. The inner calibration track would be situated on the right side of the image.

and two magnets inside the source allows us to determine the status of the source and reproduce its position when deployed within a few millimeters. A special sequence in the readout of the magnetic sensors gives feedback to the experiment control if the source is deployed, in deployment, retracted or in retraction.

Sources are stored in mirror tracks behind the last magnet sensor at the outer end of the calibration system plate. This mirror track, made of the same PTFE tubing as the other parts of the track, is wound similarly to the track inside the shield, thereby “mirroring” the shape of the deployed source as it is stored. It is possible to access this part of the calibration system and to exchange the whole mirror track with the source inside if another calibration source needs to be used. In the final configuration the  $^{228}\text{Th}$  is installed as standard source. It can be exchanged with the  $^{60}\text{Co}$  line source if additional commissioning is needed.

### 3.4. System controls

The sensors attached to the Arduino controller and the motor can be controlled individually via the data acquisition (DAQ) software ORCA [15] in an expert mode which allows debugging and tests. Non-expert users can use an interface with reduced functionality on the DAQ machines. The latter approach can start a calibration of the modules with a mouse click with automated control of calibration run duration, run-bit settings indicating a calibration run and supervision of the DAQ during deployment, calibration, and retraction of the sources.

### 3.5. Interference and background contribution

The copper cross-arm of the cryostat delivers the pumping and cooling power to the cryostat, but therefore also provides a direct line-of-sight through the lead shield to the detectors. The track was designed so that the source would not lie in this line-of-sight when placed in its storage position. While going through the outer layers of lead, the track is curved. The mirror track itself is coiled vertically so that the source in storage is

<sup>4</sup>Infineon TLE4905L E6433

<sup>5</sup><https://www.arduino.cc/en/Main/Products>



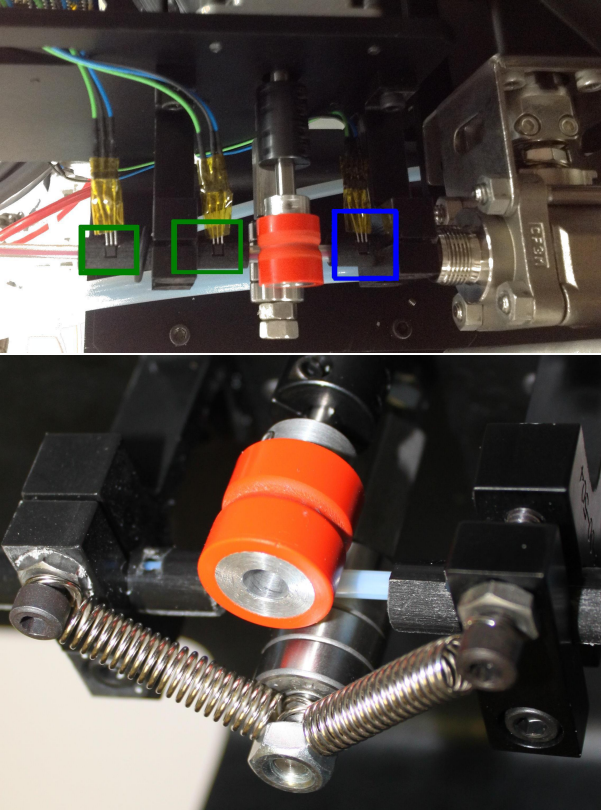


Figure 5: Radioactive line source between the two drive rollers. Two magnet sensors are placed in front of the drive roller (green boxes, left side in the upper figure). One magnet sensor is located between drive roller and the gate valve on the right (blue box). In the lower figure can be seen the springs that pull the idler pulley against the drive pulley above. In both figures the shielding and the cryostat are on the right side of the figures.

located below the cross-arm. Tests with button sources at certain locations behind the shield have verified that a source in storage does not contribute to the background of the MAJORANA DEMONSTRATOR.

We considered the possibility of removable contamination from sources being carried into or left inside the tube next to the cryostat. The mirror tracks and the cover of the system create an extra shielding so that direct contact to the sources due to ongoing lab work is avoided and line sources stay clean. In addition, the line sources, part of the tracks, and drive rollers are wiped on a regular basis and have not shown abrasion or any signs of dirt. During the last year of running we have not found any increase of backgrounds attributable to the calibration source.

#### 4. Commissioning and performance

During commissioning, a stress test of the system was performed. Calibration sources were deployed and retracted about a hundred times without any incident. Assuming a weekly calibration over the expected 5-year lifetime of the MAJORANA DEMONSTRATOR the number of operational cycles is about in the same order. The software was tested and different failure or mishandling modes were investigated. An operational procedure was written.

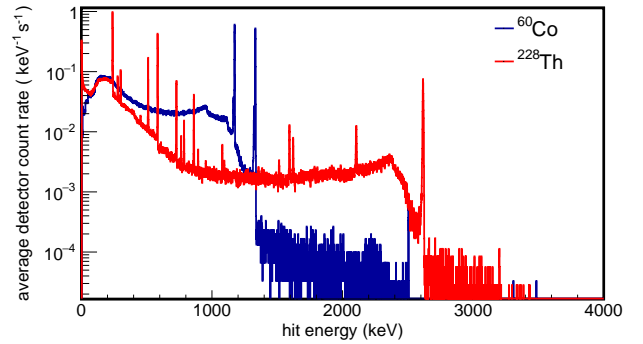


Figure 6: Single-detector energy spectrum of Module 1, averaged over the number of detectors and with a calibration time of an one hour-long data set. The spectra are shown for the detectors biased at the time of the measurement.

Figure 6 is taken from a data set from 2015 in which the first module was situated inside the shielding. In this data set, detectors in Module 1 were calibrated using its line sources. A spectrum with several peaks at different energies is available for calibration. Fig. 7 shows the integral count rate for energies between 20 and 4000 keV. The average count rate for calibrations with the  $^{60}\text{Co}$  and the  $^{228}\text{Th}$  source is around 40 Hz and 30 Hz, respectively. This fulfils the requirement on the maximum count rates discussed before. The figure shows that several detectors closer to the line source path have higher rates, as expected. Detectors at the inside or further away from the path have slightly lower rates. However, the built geometry reached the goal to have a balanced count rate within the array.

Of course, a deployed source around one module can be seen by detectors in the second cryostat. The recorded spectra in these detectors can be used to test stability. However, the count rate is not sufficient for a full calibration. For a full calibration data set of one module, a dedicated deployment of the corresponding source is necessary. In addition, it is possible to deploy both sources at the same time for high-rate data tests.

Calibration measurements are also used as a reference for our simulation campaign. The simulations using the Geant4-based framework MA<sub>GE</sub> [16, 17] are compared to measurements in order to validate the implementation of the geometry. Various parameters like the height-ratio between the full-energy peaks, the full-energy peak to Compton continuum ratio and multiplicity distributions are affected by the positioning of the source relative to the detectors as well as by the amount of material located between source and detectors. Using the calibration measurements, the transition layer of the models in the simulations can be validated. The size of the transition layer affects the size of the step function under a full-energy peak which is necessary to get similar spectral shape. A first analysis showed that MA<sub>GE</sub> is able to describe the measured spectra in calibration runs very well, as shown in Fig. 8. The simulation is in very good agreement and can be used to build up a pulse-shape library, to study the efficiency of cuts and the background in general.

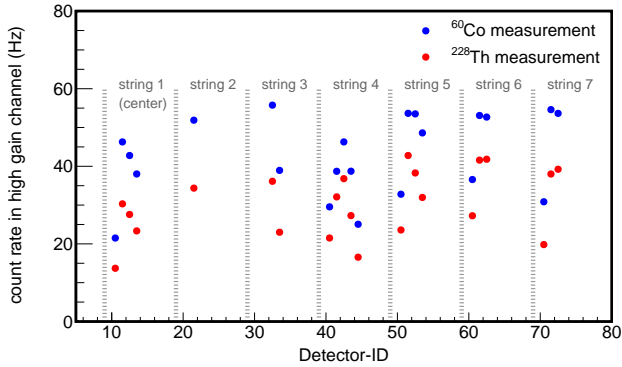


Figure 7: Integral count rate per detector in the high gain channel between 20 and 4000 keV for the two installed line sources. The count rate is given for the detectors used for the first data set of Module 1.

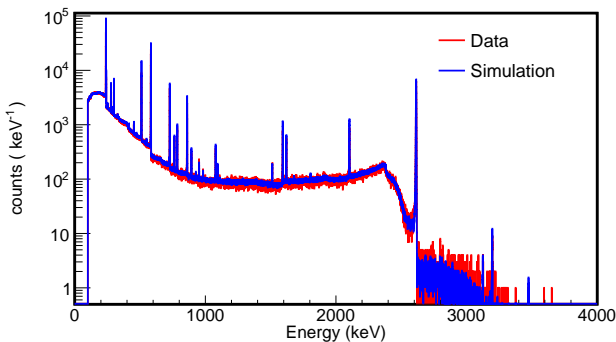


Figure 8: Comparison of a  $^{228}\text{Th}$  line source simulation using MA GE and a measurement of Module 1. The simulated distribution was normalized by matching the integrals of both curves in the range from 2595 keV to 2635 keV.

## 5. Summary

A calibration system has been designed for the MAJORANA DEMONSTRATOR. The system has to fulfil special requirements in terms of cleanliness, stable positioning and reproducibility. The strength of the radioactive source was adjusted to the special needs of the data stream and ensures stable data taking. Two systems, one for each cryostat in the shield, were built. The systems deploy radioactive sources from outside the shielding to a position next to the detectors so that energy calibrations and other studies are possible. In contrast to other systems, our line source approach can calibrate the whole array at the same time without moving the source. The results can be used to study the agreement of coincidences in experiment and simulation. The design, using a line source in which the radioactivity is distributed along a certain length, ensures a sufficient count rate in all detectors of the array so that one calibration run can be used for all detectors of a module. Also, it has been shown that the calibration system around one module can easily be copied, which is important for the scalability of such a modular approach when going to ton-scale experiments. Both systems are operated remotely and the controls are implemented in the DAQ system of the MAJORANA DEMONSTRATOR. While the exact design depends on the future experimental conditions, the MJD

calibration system shows that it is possible to construct a system using easily accessible materials, sensors and readout electronics while still holding to all cleanliness and low-background limits.

## 6. Acknowledgements

This material is based upon work supported by the U.S. Department of Energy, Office of Science, Office of Nuclear Physics under Award Numbers DE-AC02-05CH11231, DE-AC52-06NA25396, DE-FG02-97ER41041, DE-FG02-97ER41033, DE-FG02-97ER41042, DE-SC0012612, DE-FG02-10ER41715, DE-SC0010254, and DE-FG02-97ER41020. We acknowledge support from the Particle Astrophysics Program and Nuclear Physics Program of the National Science Foundation through grant numbers PHY-0919270, PHY-1003940, 0855314, PHY-1202950, MRI 0923142 and 1003399. We acknowledge support from the Russian Foundation for Basic Research, grant No. 15-02-02919. We acknowledge the support of the U.S. Department of Energy through the LANL/LDRD Program. This research used resources of the Oak Ridge Leadership Computing Facility, which is a DOE Office of Science User Facility supported under Contract DE-AC05-00OR22725. This research used resources of the National Energy Research Scientific Computing Center, a DOE Office of Science User Facility supported under Contract No. DE-AC02-05CH11231. We thank our hosts and colleagues at the Sanford Underground Research Facility for their support.

## References

- [1] F. T. Avignone III, et al., Double beta decay, MAJORANA neutrinos, and neutrino mass, *Rev. Mod. Phys.* 80 (2008) 481–516, URL <http://link.aps.org/doi/10.1103/RevModPhys.80.481>.
- [2] J. D. Vergados, et al., Theory of neutrinoless double-beta decay, *Reports on Progress in Physics* 75 (10) (2012) 106301, URL <http://stacks.iop.org/0034-4885/75/i=10/a=106301>.
- [3] H. V. Klapdor-Kleingrothaus, I. V. Krivosheina, The evidence for observation of  $0\nu\beta\beta$  decay: the identification of  $0\nu\beta\beta$  events from the full spectra, *Modern Physics Letters A* 21 (20) (2006) 1547–1566, URL <http://www.worldscientific.com/doi/abs/10.1142/S0217732306020937>.
- [4] EXO-200-Collaboration, Search for MAJORANA neutrinos with the first two years of EXO-200 data, *Nature* 510 (7504) (2014) 229–234, ISSN 0028-0836, URL <http://dx.doi.org/10.1038/nature13432>.
- [5] M. Agostini, et al., Search of Neutrinoless Double Beta Decay with the GERDA Experiment, *Nuclear and Particle Physics Proceedings* 273275 (2016) 1876 – 1882, ISSN 2405-6014, URL <http://www.sciencedirect.com/science/article/pii/S2405601415007920>, 37th International Conference on High Energy Physics (ICHEP).
- [6] Search for Majorana Neutrinos Near the Inverted Mass Hierarchy Region with KamLAND-Zen, *Phys. Rev. Lett.* 117 (2016) 082503, URL <http://link.aps.org/doi/10.1103/PhysRevLett.117.082503>.
- [7] A. G. Cohen, D. B. Kaplan, A. E. Nelson, Progress in electroweak baryogenesis, *Ann. Rev. Nucl. Part. Sci.* 43 (1993) 27–70.
- [8] N. Abgrall, et al., The MAJORANA DEMONSTRATOR Neutrinoless Double-Beta Decay Experiment, *Advances in High Energy Physics* 2014 (2014) 1–18, URL <http://dx.doi.org/10.1155/2014/365432>.
- [9] R. Cooper, et al., A Pulse Shape Analysis technique for the MAJORANA experiment, *Nuclear Instruments and Methods in Physics Research Section A: Accelerators, Spectrometers, Detectors and*

Associated Equipment 629 (1) (2011) 303 – 310, ISSN 0168-9002, URL <http://www.sciencedirect.com/science/article/pii/S0168900210024915>.

- [10] S. Mertens, et al., MAJORANA Collaboration's Experience with Germanium Detectors, *Journal of Physics: Conference Series* 606 (1) (2015) 012005, URL <http://stacks.iop.org/1742-6596/606/i=1/a=012005>.
- [11] S. Agostinelli, et al., Geant4 a simulation toolkit, *Nuclear Instruments and Methods in Physics Research Section A: Accelerators, Spectrometers, Detectors and Associated Equipment* 506 (3) (2003) 250 – 303, ISSN 0168-9002, URL <http://www.sciencedirect.com/science/article/pii/S0168900203013688>.
- [12] M. Boswell, et al., Overview of calibration design, Tech. Rep., MAJORANA internal report, 2010.
- [13] N. Abgrall, et al., The MAJORANA Demonstrator radioassay program, *Nuclear Instruments and Methods in Physics Research Section A: Accelerators, Spectrometers, Detectors and Associated Equipment* 828 (2016) 22 – 36, ISSN 0168-9002, URL <http://www.sciencedirect.com/science/article/pii/S0168900216302832>.
- [14] L. Baudis, et al., Monte Carlo studies and optimization for the calibration system of the GERDA experiment, *Nucl. Instrum. Meth. A* 729 (2013) 557–564, URL <http://www.sciencedirect.com/science/article/pii/S0168900213011273>.
- [15] M. A. Howe, et al., Sudbury Neutrino Observatory Neutral Current Detector Acquisition Software Overview, *IEEE Trans. Nucl. Sci.* 51 (2004) 878–883.
- [16] M. Bauer, et al., MaGe: a Monte Carlo framework for the GERDA and MAJORANA double beta decay experiments, *Journal of Physics: Conference Series* 39 (1) (2006) 362, URL <http://stacks.iop.org/1742-6596/39/i=1/a=097>.
- [17] M. Boswell, et al., MaGe - a Geant4-based Monte Carlo Application Framework for Low-background Germanium Experiments, arXiv preprint nucl-ex URL <https://arxiv.org/abs/1011.3827v1>.